

# The Localized Corrosion of Al 6XXX Alloys

B.A. Shaw, M.M. McCosby, A.M. Abdullah, and H.W. Pickering

This paper presents some recent findings on localized corrosion with a focus on Al 6XXX alloys and on the current times resistance (IR) voltage that exists between the separated anodic and cathodic reactions. Some newly developed concepts help quantify the relationship between the IR voltage and the polarization curve that exists on the crevice wall, thereby providing for a deeper understanding on how crevice corrosion occurs in many metals and alloys. A signature of the IR voltage form of crevice corrosion in metal/electrolyte systems is the existence of an active/passive transition in their polarization curves. An aluminum/electrolyte system has been found to undergo this form of crevice corrosion. Some new results on intergranular corrosion in Al 6XXX alloys are also presented.

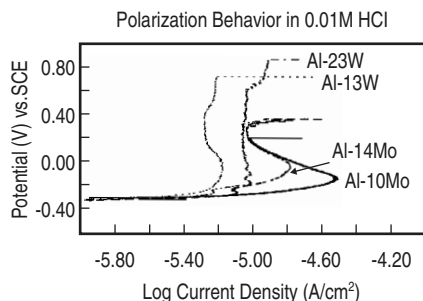


Figure 1. Anodic polarization behavior of nonequilibrium Al-Mo and Al-W alloys in 0.01 M HCl, illustrating the active peaks observed in the Al-10% Mo and Al-14% Mo alloys.

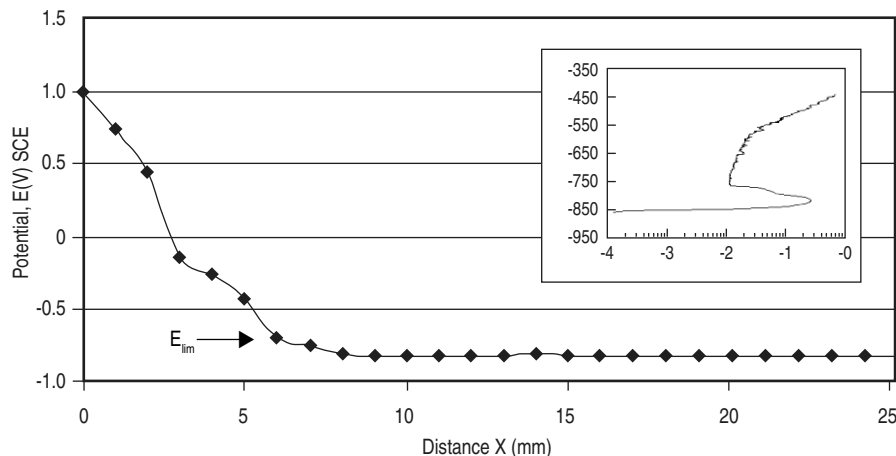


Figure 2. In-situ measured  $E(x)$  profile on the crevice wall during crevice corrosion of Al 6XXX alloy (0.68% Cu) in a saturated solution of NaCl + 1 mM  $\text{NH}_4\text{NO}_3$  at 90°C. The applied potential was 1 V<sub>SCE</sub>. Insert shows the polarization curve (with  $E_{oc} = -850 \text{ mV}_{SCE}$  aligned with  $E_{lim} = -0.85 \text{ V}_{SCE}$  of the  $E(x)$  profile).

## INTRODUCTION

Current times resistance (IR) voltage plays a major role in the operation of local corrosion cells. This voltage drop is responsible for the existence on the cavity's walls of the system's polarization curve, including its active peak. This  $E(x)$  distribution on the walls is the basis of the IR mechanism that links the corrosive attack occurring at a particular location of the cavity's walls with  $E(x)$  values that are in the active peak region of the cavity solution's polarization curve. The IR voltage within the cavity's electrolyte is generated by the ionic current,  $I$ , that flows between the anodic reaction inside the cavity and the cathodic reaction at another location, either within the cavity closer to its mouth or on the outer surface (during open-circuit corrosion) or at the counter electrode (during external anodic polarization of the sample).

## CREVICE CORROSION IN ALUMINUM 6XXX ALLOYS

The IR mechanism of crevice corrosion has been shown to operate in spontaneously active systems (iron/steel,<sup>4-6</sup> nickel,<sup>7,8,12</sup> and stainless steel<sup>9,10</sup>) and has been proposed to occur in some corrosion resistant, spontaneously passive alloys.<sup>13,14</sup> Unlike the acidification mechanism, which attributes crevice corrosion solely to changes in crevice solution composition,<sup>15-18</sup> the IR mechanism relates crevice corrosion to the IR voltage drop and resulting shift of the electrode potential on the crevice wall,  $E(x)$ , into the active region of the system's polarization curve, as mentioned in the highlighted text (Figure A). Acidification within the crevice, and certain other solution composition changes, can modify the anodic polarization curve that exists on the crevice wall. Particularly affected is the size of its active peak, or an active peak can form and grow in the case of spontaneously passive metal/electrolyte systems.<sup>1,7,9,13,14</sup> Evidence of active dissolution peaks in the anodic polarization curves for nonequilibrium Al-W and Al-Mo alloys exposed to a 0.01M HCl solution has been given by Principe and are presented in Figure 1.<sup>19</sup>

The forms of experimental data that show the stabilization of crevice corrosion by the IR mechanism include all of the following:

- The direct measurement of a large  $E(x)$  profile on the crevice wall, which is independently confirmed under constant or increasing pH conditions by the observation of an increased HER rate on the crevice wall
- The good match between the directly measured electrode potential,  $E(x)$ , bounding the corrosively attacked wall region and the  $E$  region of the active peak in the polarization curve
- The two latter observations under conditions of a constant polarization curve on the crevice wall (constant composition of the crevice electrolyte as a result of convective mixing with the bulk electrolyte) that could be verified by measurement of a constant  $E_{pass}$  at  $x_{pass}$  on the crevice wall

The above forms of data are clearly evident in all of the spontaneously active systems studied to date, including the recently studied corrosion-resistant alloys, aluminum 6XXX alloy and alloy T-2205 duplex stainless steel. Following are the results for aluminum 6XXX; results for alloy T-2205 duplex stainless steel can be found elsewhere.<sup>9,10</sup>

- The immediate onset of crevice corrosion (for  $AR > AR_c$ ; see highlighted text for definitions) with no change in solution composition
- Several behaviors observed during crevice corrosion that have been found to be characteristic of the IR voltage form of crevice corrosion.

The above forms of data are clearly evident in all of the spontaneously active systems studied to date, including the recently studied corrosion-resistant alloys, aluminum 6XXX alloy and alloy T-2205 duplex stainless steel. Following are the results for aluminum 6XXX; results for alloy T-2205 duplex stainless steel can be found elsewhere.<sup>9,10</sup>

To provide the types of experimental

data mentioned previously, an alloy/electrolyte system's polarization curve must contain a large active peak and relatively low passive current. Then, crevice corrosion will immediately occur in a crevice of small AR that can be readily constructed in the laboratory with a relatively large opening/gap dimension (e.g.,  $a = 0.05$  cm). In this case, the measuring probes can readily be inserted into the crevice for easy and reproducible data collection. However, in contrast to most other alloys, such as the stainless steels, titanium alloys, steels, and nickel, aluminum alloys do not exhibit active peaks in their polarization curves in the vast majority of environments, even when a simulated crevice solution is used as the bulk electrolyte for the polarization curve determination. An active peak is seen in an occasional aluminum/electrolyte system. More often, transient active peaks are seen under fast potential scan conditions. In order to test for the IR form of crevice corrosion in aluminum, some of the previously mentioned types of measurements were performed for both categories (stable and transient) of active peak in aluminum/electrolyte systems.

Data have been obtained for an Al 6XXX alloy in two different environments: one in which the alloy exhibits a stable active peak in the polarization curve (Al 6XXX/saturated NaCl at 90°C) and, the other, a transient active peak in the polarization curve (Al 6XXX/NaNO<sub>3</sub>, pH 2 to 5.4, at room temperature). In the latter system, the local pH is first increased by a cathodic pretreatment of hydrogen evolution. A fast (as opposed to the normal slow) scan in the oxidation direction will then show an active peak for this system.

Crevice-corrosion experiments were carried out for the NaCl solution at 90°C by anodic polarization into the passive region. However, the sample in the HNO<sub>3</sub> (pH 1) solution at room temperature was polarized cathodically rather than anodically. Both systems yielded large (measured) IR voltages in the crevice electrolyte. The experimental details and more complete description of the results are presented elsewhere.<sup>20</sup>

For the NaCl solution at 90°C, stable crevice corrosion immediately occurred under conditions of a constant (saturated) chloride-ion concentration, with the same features illustrated in Figure B. The  $E(x)$  profile was similar to that of the previously studied alloys that were found to be susceptible to the IR form of crevice corrosion (Figure 2).

For the HNO<sub>3</sub> (pH 1) solution and cathodic polarization of the sample,  $E(x)$  increased to more noble, rather than less noble, values with increasing distance into the crevice (since the net current,  $I$ , was flowing into the crevice, opposite to that for anodic polarization). Crevice corrosion was observed on the wall partway into the crevice, similar to that for anodic polarization shown in Figure B (but without the pitting corrosion region since  $E(x)$  values can not shift during cathodic polarization beyond the pH-dependent open circuit potential,  $E_{oc}$ , established by the hydrogen evolution and aluminum-dissolution reactions<sup>1</sup>). Figure 3 is a micrograph of the crevice wall in the region of the cathodic-to-active transition,  $x_{act}$ , showing the  $x_{act}$  boundary with the  $E(x)$  profile (not shown) measured in-situ at four hours of crevice corrosion, after which the experiment was stopped and the micrograph in Figure 3 was taken. Based on Figure 3 and IR theory, hydrogen evolution solely occurs on the crevice wall above the boundary,  $x_{act}$ , the anodic (active aluminum) dissolution region ( $x_{act} \leq x \leq x_{pass}$ ) occurs between the  $x_{act}$  and  $x_{pass}$  boundaries, and the passive region exists below the  $x_{pass}$  boundary (at  $x \geq x_{pass}$ ), as shown in the schematic of Figure 3.

Preliminary data indicate that the  $E(x)$  values on the crevice wall in the region of

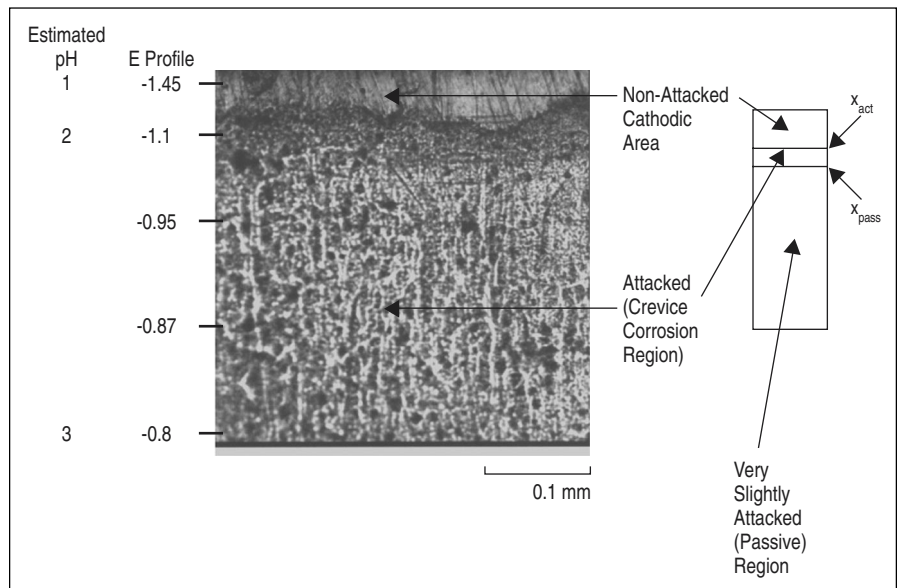


Figure 3. Micrograph in the vicinity of the  $x_{act}$  boundary (and schematic of the crevice wall) for an Al 6XXX alloy that was cathodically polarized at  $-1.45$  V<sub>SCE</sub> for four hours in 0.1 M HNO<sub>3</sub>. The cathodically protected region is above  $x_{act}$  and the crevice corrosion region is below  $x_{act}$  on the crevice wall.

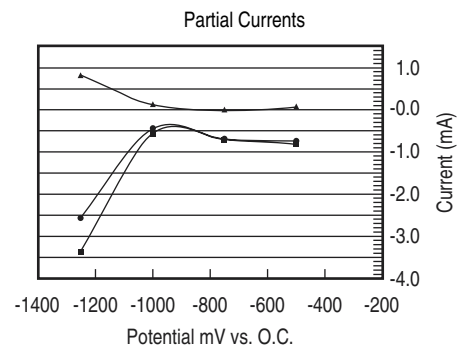


Figure 4. ▲—Partial polarization curve for Al 6XXX alloy in 0.01M HCl. ●—Measured (net) polarization curve. ■—Partial polarization curve for the hydrogen evolution reaction.

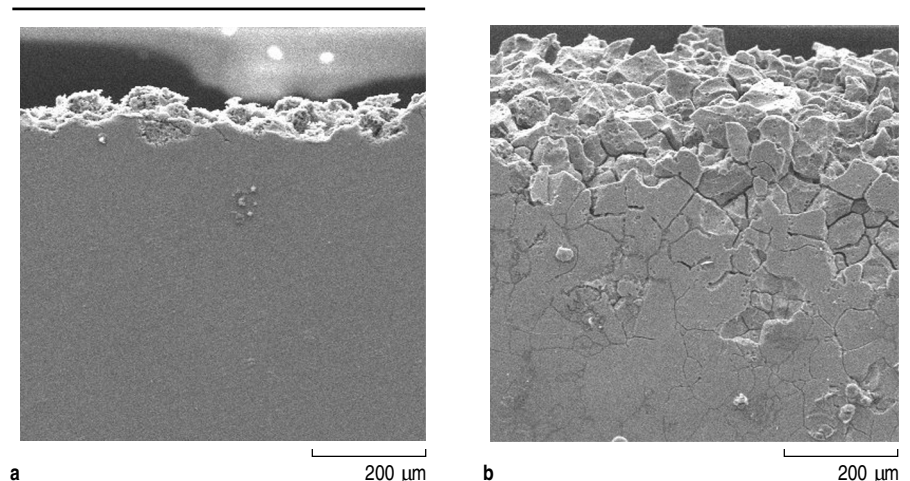


Figure 5. SEM micrographs after polarization for several days at  $-300$  mV<sub>SCE</sub> illustrating the differences between (a) the uniform dissolution of the Al 6XXX alloy and (b) the dominant intergranular attack of an Al 6XXX alloy containing 1.5%Cu.

the corrosive attack seen in Figure 3 were in the range of the  $E$  values for the active peak seen in the fast-scan polarization curve (not shown). If these data are confirmed, [e.g., if the  $E_{act}$  value, which is measured at  $x_{act}$  on the crevice wall (Figure 3) is  $\cong -1 V_{SCE}$ , it would be close to the value on the polarization curve, which was  $E = -1.1 V_{SCE}$  for a pH 2 solution], it will mean that an IR voltage of approximately 0.4 V was required for there to be  $E(x)$  values on the crevice wall that corresponded to the active peak of the polarization curve. Alternatively, if the  $E_{act}$  value measured on the crevice wall (at  $x_{act}$ ) is much more negative (i.e., close to the applied potential,  $E_{x=0} = -1.45 V_{SCE}$ , rather than close to the  $E_{act}$  value of the polarization curve), the IR voltage would not be important in the stabilization process.

Preliminary current-time data indicate that the crevice-corrosion process revealed in Figure 3 started at some time after the cathodic polarization but less than 1.5 hours into the experiment. During the induction period prior to the start of crevice corrosion, hydrogen evolution within the crevice is expected to cause a rise in the local pH and breakdown of the passive film and, hence, formation of the active peak in the

## ROLE OF IR THEORY IN LOCALIZED CORROSION

When metal/electrolyte systems with active/passive transitions in their polarization curves (spontaneously active systems) are anodically polarized into the passive region, the passivation process begins on the outer surface, but may then progress only part way into the crevice. In this case a large anodic current continues to flow through the crevice electrolyte to the cathodic reaction. This is the ionic current that produces the IR voltage and resulting  $E(x)$  profile and current distribution,  $i(x)$ , on the crevice wall (Figure A).<sup>1,2</sup> Although the  $E(x)$  profile tends to be linear on the passive section of the crevice wall, it is nonlinear on the active section where  $I$  decreases with increasing  $x$ .<sup>2,3</sup> As a result, the polarization curve that exists on the crevice wall is skewed with respect to the potential on the  $x$  axis (Figure A). Since the existence of the  $E(x)$  distribution on the crevice wall is instantaneous with the onset of the ionic current, crevice corrosion occurs immediately (i.e., without an induction period) in crevices of sufficiently large aspect ratio (AR) (depth,  $L$ , divided by the opening dimension,  $a$ , of the crevice), in spontaneously active systems.<sup>2</sup> Since, in this case, there is no time prior to the start of crevice corrosion for the solution composition to change, the immediate onset of crevice corrosion is a proof that the  $E(x)$  profile (with values in the active peak region of the polarization curve) is responsible for the initial stabilization of the crevice-corrosion process.

For the IR voltage form of crevice corrosion (with or without change in the composition of the crevice solution), the following characteristic features are observed: The transition from passive to active dissolution on the crevice wall occurs at a distance,  $x_{pass}$  (Figure A) where the electrode potential,  $E_{pass}$ , on the crevice wall equals the potential of the passive/active transition in the polarization curve for the crevice solution. The  $x_{pass}$  boundary can be straight and perpendicular to the  $x$  axis for one-dimensional crevices (i.e., for crevices open to the electrolyte only at  $x=0$ ), although gaseous (typically hydrogen) and solid corrosion products in the cavity's electrolyte typically distort this boundary.<sup>4-7</sup> These corrosion products can be removed by purging the crevice electrolyte with fresh bulk solution in order to restore the regularity of the  $x_{pass}$  boundary and of the  $E(x)$  profile. Purging works best for crevices in the upside-down orientation for which gravity facilitates the convective mixing of the crevice and bulk solutions.<sup>7-10</sup> A measure of how well the purging also maintains a constant electrolyte composition within the crevice and, hence, a constant polarization curve on the crevice wall during the crevice corrosion process, is the constancy of the measured  $E_{pass}$  value at  $x_{pass}$  on the crevice wall. In well-mixed crevice electrolytes, constant  $E_{pass}$  values ( $\pm 5$  mV) have been measured during crevice corrosion processes lasting tens of hours.<sup>8-10</sup> This convective mixing

action also eliminates the solution composition as a variable, and, as such, the  $E(x)$  potential profile can be conclusively shown to be the stabilizing force not only for the initiation of crevice corrosion, but also for its continuation.

Figure B is a typical experimental result (in-situ photograph taken through the Plexiglas) showing the features in Figure A, including the  $x_{pass}$  boundary and the region of corrosive attack below  $x_{pass}$ . It also reveals a region of pitting corrosion ( $0 \leq x \leq E_{m0}$ ) at the mouth of the crevice, a consequence of an applied  $E_{x=0}$  value that was more positive than the pitting potential in this experiment. The hydrogen gas bubble formation inside the crevice, observed through the Plexiglas, is schematically indicated in Figure Bb. In-situ observation of the  $H_2$  bubbles during the ongoing crevice-corrosion process is independent proof that an (often necessarily large) IR voltage and  $E(x)$  profile exist in the crevice, since it is only in this way under constant or increasing pH conditions that  $E(x)$  could be more negative than the equilibrium potential,  $E_{rev}$ , of the hydrogen evolution reaction (HER). During IR-induced crevice and pitting corrosion, large  $E(x)$  profiles on the crevice walls are also routinely measured using a microprobe reference electrode.<sup>4-11</sup> These same features of IR-induced crevice corrosion can also exist inside pits, stabilize their growth,<sup>11</sup> and even be responsible for the transition from metastable to stable pit formation.<sup>6</sup>

The location of  $x_{pass}$  on the crevice wall is observed to move towards the crevice mouth during crevice corrosion, a consequence of an increasing  $dE(x)/dx$  with time since the ionic current,  $I$ , increases with time as the exposed wall area increases over the geometrical wall area.<sup>4-10</sup> Hence, the penetration profile on the crevice wall extends over more of the crevice wall with time of stable crevice corrosion. This motion of  $x_{pass}$ , as well as the wall locations of the peak currents, to smaller  $x$  values with time as shown in Figure C, tends to extend the penetration profile toward the mouth ( $x=0$ ) of the crevice and to suppress the large variations of the current density in the active peak of the polarization curve. The current can also increase (or decrease) if the size of the active peak changes as a result of changes in solution composition when stagnation of the crevice electrolyte occurs (in the absence of convective mixing).

A given opening dimension,  $a$ , has a critical depth,  $L_c$ , below which the crevice will not support a crevice-corrosion process for a given bulk solution composition. In this event (i.e.,  $L < L_c$ ), crevice corrosion could eventually occur if the composition of the crevice solution changes from that of the bulk solution during an induction period. This composition change would have to increase the size of the active peak of the crevice solution's polarization curve, as typically occurs for a decrease in pH and/or increase in the chloride-ion concentration. On the other hand, increases in pH that occur for low-pH solutions (for which the hydrolysis reaction cannot occur) and increases in the metal-ion concentration have the opposite effect, decreasing the

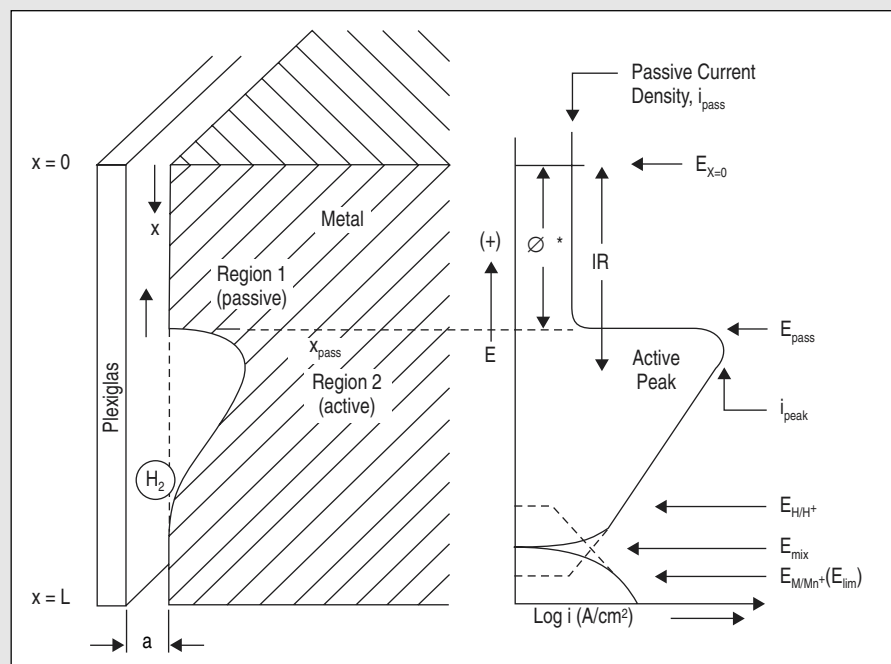


Figure A. Schematic illustrations of the crevice corrosion attack on the crevice wall (left), and the IR-produced  $E(x)$  distribution and resulting  $i(x)$  current densities (skewed polarization curve) on the crevice wall (right).

polarization curve that exists on the crevice wall. The IR voltage could also prolong the induction period. Because the HER rate decreases as the IR voltage increases, causing the rise in pH to take longer.

These results for the first system (NaCl, 90°C), and to a lesser degree for the second system (HNO<sub>3</sub>, room temperature), are support for crevice corrosion by the IR mechanism. Still, these systems could be special cases since, in contrast to most aluminum/electrolyte systems, they exhibit either stable or transient active peaks in their polarization curves. Nevertheless, active peaks may be present in other systems since much of the aluminum partial polarization curve is masked by the cathodic hydrogen evolution reaction. Partial current measurements, in which hydrogen gas is collected during the course of cathodic polarization measurements, reveal the active dissolution behavior of Al alloys.<sup>21</sup> Such measurements were conducted on 6XXX alloys in 0.01M HCl. The active dissolution behavior for the Al 6XXX alloy is evident once the amount of hydrogen is converted into a current and subtracted from the measured polarization curve, as shown in Figure 4.

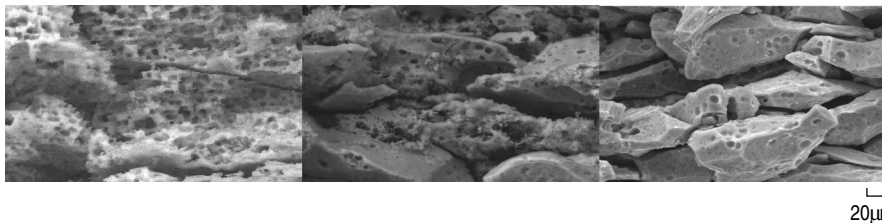


Figure 6. SEM micrograph showing the degree of intragranular and intergranular attack for the Al 6XXX alloys with and without copper: (left) 0% copper, (middle) 0.7% copper, and (right) 1.5% copper.

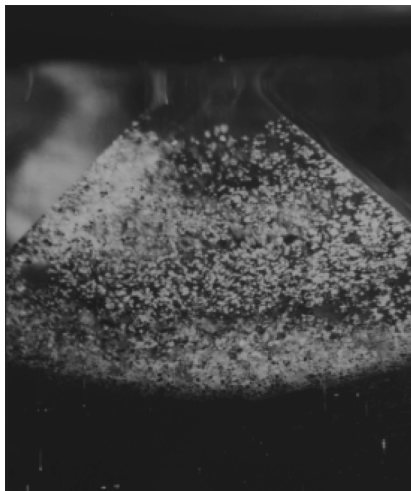


Figure 7. Optical micrograph of a pencil-type electrode after several days of polarization at  $-0.300 \text{ mV}_{\text{SCE}}$  showing a large number of detached grains resulting from intergranular attack of the Al 6XXX alloy surface.

B.A. Shaw and M.M. McCosby are with the Department of Engineering Science and Mechanics, and A.M. Abdullah and H.W. Pickering are with the Department of Materials Science and Engineering at The Pennsylvania State University.

For more information, contact B.A. Shaw, The Pennsylvania State University, Department of Engineering Science and Mechanics, University Park, Pennsylvania 16802; (814) 865-7828; fax (814) 865-0122; e-mail bas13.psu.edu.

## GRAIN BOUNDARY CORROSION IN ALUMINUM 6XXX ALLOY

Anodic polarization of copper-containing Al 6XXX alloys at  $-300 \text{ mV}_{\text{SCE}}$  in 0.05 M HCl causes intergranular corrosion (IGC) with substantial hydrogen gas evolution within the intergranular grooves. Without added copper, the corrosive attack in the Al 6XXX alloy is largely uniform with substantial intra-

granular (localized crystalline) attack of the alloy (presumably associated with the  $\text{Mg}_2\text{Si}$  precipitates in the microstructure). With increasing copper concentration, the degree of intragranular attack diminishes and the degree of intergranular attack increases (Figures 5–6). Intergranular attack under these highly polarized conditions ( $E = -0.3 \text{ V}_{\text{SCE}}$ ) penetrated 1–2 mm into the alloy (after several hours of polarization) and a large number of detached grains were noticed within the confines of a pencil-type electrode cell (Figure 7). Intergranular corrosion is also noted under open-circuit conditions for the copper-containing Al 6XXX alloys exposed to chloride-containing environments; however, penetration depths are much lower.

Since a net current is measured between the anodic aluminum dissolution at the advancing front of the grain boundary penetration and the cathodic reaction on the counter electrode, IR voltage and  $E(x)$  and  $i(x)$  distributions on the walls of the grain boundary penetrations can be concluded to exist just as in the case of the crevice walls described above. The observed increased rate of hydrogen evolution inside the grain boundary penetration (relative to the outer surface) is also a proof of the existence of this IR voltage when the applied potential is more positive than the standard potential of the HER, as was the case in some of these experiments. One of the consequences of the IR voltage would be the occurrence of corrosive penetration into the neighboring grains if an active peak forms in the polarization curve existing on the walls of the grain boundary grooves, similar to the corrosive attack observed inside grain boundary grooves that formed in sensitized stainless steel.<sup>22</sup>

## ACKNOWLEDGEMENTS

Thanks to Alan Shi for performing some of the microscopy, and to Ela Sikora and Janusz Sikora for their helpful discussions. This work was sponsored by Alcoa, Inc.

## References

1. H.W. Pickering, *Corros. Sci.*, 29 (1989), p. 325; *Corrosion*, 42 (1986), p. 125; *Corrosion and Corrosion Protection*, The Electrochemical Society Softbound Series, 81-8 (1981), pp. 85–91.
2. Y. Xu and H.W. Pickering, *J. Electrochem. Soc.*, 140 (1993), p. 658.
3. B.G. Ateya, M.I. Abdulsalam, and H.W. Pickering, *Proc. Symp. in Honor of Prof. N. Sato: Passivity and Localized Corrosion*, PV 99-27 (Pennington, NJ: The Electrochem. Soc., 2000), pp. 599–608.
4. A. Valdes and H.W. Pickering, *Advances in Localized Corrosion*, ed. H. Isaacs et al. (Houston, TX: NACE, 1990), p. 393; K. Cho, *J. Electrochem. Soc.*, 137 (1990), p. 3313; E. Nystrom et al., *J. Electrochem. Soc.*, 141 (1994), p. 358; K. Cho, M. I. Abdulsalam, and H. W. Pickering, *J. Electrochem. Soc.*, 145 (1998), p. 1862.
5. K. Cho and H.W. Pickering, *J. Electrochem. Soc.*, 138 (1991), p. 156.
6. Y. Xu, M. Wang, and H.W. Pickering, *J. Electrochem. Soc.*, 140 (1993), p. 3448.
7. M. Wang, H.W. Pickering, and Y. Xu, *J. Electrochem. Soc.*, 142 (1995), p. 2986.
8. M.I. Abdulsalam and H.W. Pickering, *Corros. Sci.*, 41 (1999), p. 351; M.I. Abdulsalam and H.W. Pickering, *J. Electrochem. Soc.*, 145 (1998), p. 2276.
9. J.N. Al-Khamis and H.W. Pickering, *Chemistry and Electrochemistry of Corrosion And Stress Corrosion Cracking: A Symposium Honoring the Contributions of R. W. Staehle* (Warrendale, PA: TMS, 2001), pp. 319–337; J.N. Al-Khamis and H.W. Pickering, *7th Int. Symp. on Electrochemical Methods in Corrosion Research*, EMCR'2000, CD-ROM (Budapest, Hungary: Chemical Research Center of the Hungarian Academy of Sciences, 2000).
10. J.N. Al-Khamis and H.W. Pickering, *J. Electrochem. Soc.*, to be published.
11. H.W. Pickering and R.P. Frankenthal, *J. Electrochem. Soc.*, 119 (1972), p. 1297.
12. L.A. DeJong and R.G. Kelly, *Critical Factors in Localized Corrosion III*, vol. 98-17, ed. R.G. Kelly et al. (Pennington, NJ: The Electrochem. Soc., 1999), p. 678.
13. B.A. Shaw, P.J. Moran, and P.O. Gartland, *Corrosion Sci.*, 32 (1991), p. 707.
14. R.S. Lillard, M.P. Jurinski, and J.R. Scully, *Corrosion*, 50 (1994), p. 251; R.S. Lillard and J.R. Scully, *J. Electrochem. Soc.*, 141 (1994), p. 3006.
15. M.G. Fontana, *Corrosion Eng.*, 3rd Ed. (New York: McGraw-Hill Book, 1986), pp. 51–59.
16. J.W. Oldfield and W.H. Sutton, *British Corrosion Journal*, 13 (1978), p. 13.
17. H.H. Strehblow, *Werkst. Korros.*, 27 (1976), p. 792.
18. N. Sato, *J. Electrochem. Soc.*, 129 (1982), p. 260.
19. E. Principe, "An Investigation of the Enhanced Passivity Observed in Nonequilibrium Aluminum Alloys" (Ph.D. Dissertation, The Pennsylvania State University, May 1996).
20. A.M. Abdullah, B.A. Shaw, and H.W. Pickering, *Symp. on Corrosion and Corrosion Prevention of Low Density Metals and Alloys*, ed. R.G. Buchheit and B.A. Shaw (Pennington, NJ: The Electrochem. Soc., 2001).
21. S. Real, M. Urquidi-Macdonald, and D.D. Macdonald, *J. Electrochem. Soc.*, 135 (1988), p. 1633.
22. W.R. Kelly, R.N. Iyer, and H.W. Pickering, *J. Electrochem. Soc.*, 140 (1993), p. 3134.